Politecnico di Torino

Politecnico di Torino

Master of Science in Energy and Nuclear Engineering
01FJIXY - Computational Thermomechanics
A.Y. 2025/2026

Homework 07 - Cooling of a Superconducting Cable In Conduit Conductor

Tommaso COGOZZO

1 Problem statement and given data

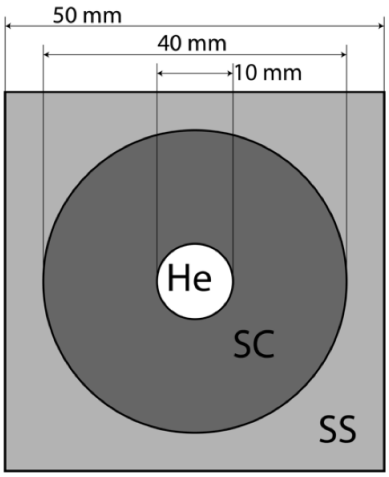

Figure 1: Cross section of a cable-in-conduit conductor (CICC) used in fusion devices

Data:

- Channel diameter : $D_h = 10\,mm$
- Cable diameter: $D_c = 40\,mm$
- Jacket size: $S_j = 50\,mm$
- SC conductivity: $k_{SC} = 10\,W/(m\,K)$
- SS conductivity: $k_{SS} = 0.2\,W/(m\,K)$
- SC heat deposition: $q_{SC} = 10\,kW/m^3$
- SS heat deposition: $q_{SS} = 7\,kW/m^3$
- Helium temperature: $T_{He} = 4.5\,K$
- SC-Helium heat transf coef: $h = 5000W/(m^2\,K)$

2 Objective

The objective of this study is to model and analyze the steady-state temperature distribution in the cross-section of a cable-in-conduit conductor (CICC) used in fusion devices. The conductor consists of a superconducting (SC) cable cooled by supercritical helium (He) and surrounded by a stainless steel (SS) jacket. The analysis accounts for volumetric heat deposition within both the SC cable and the SS jacket due to nuclear heating from the plasma, as well as convective heat transfer between the SC and helium.

To reduce the computational cost while maintaining accuracy, the inherent geometric and thermal symmetry of the problem is exploited. Specifically, only one-eighth of the total cross-sectional domain is modeled, considering appropriate symmetry boundary conditions along the horizontal and vertical axes. This approach allows for a substantial reduction in the number of finite elements required while preserving the fidelity of the temperature field.

The numerical study is conducted using the Finite Element Analysis (FEA) software FEAP, discretizing the domain with linear triangular (3-node) and rectangular (4-node) plane stress elements. The temperature distribution is evaluated for both coarse and refined meshes, and the results are presented in terms of temperature contours, heat flux distributions, and temperature profiles along symmetry axes.

3 Finite Element Analysis with 3-Nodes Triangular Elements

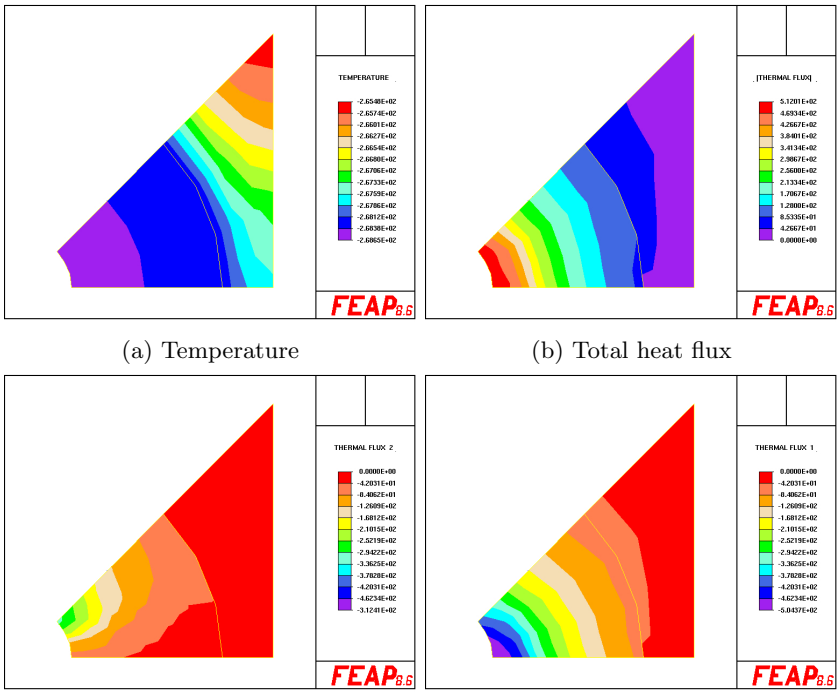

(a) Temperature

(b) Total heat flux

(c) Vertical heat flux

(d) Horizontal heat flux

Figure 2: Computed temperature and heat flux with mesh =1

The first discretization, employing three nodes triangular finite elements with a uniform mesh size equal to 1, yielded the temperature and heat flux results shown in Figures 2a and 2b, respectively. Figures 2c and 2d further report the corresponding color maps of the vertical and horizontal components of the heat flux.

At first glance, the correct implementation of the boundary conditions is clearly evident. In particular, as shown in Figure 2a, the minimum temperature attains a value of $-268.6\,^{\circ}\mathrm{C}$, which corresponds to $4.5\,\mathrm{K}$, consistently with the imposed helium temperature at the origin. Moreover, the heat flux distribution reported in Figure 2b correctly vanishes in the proximity of the right boundary of the domain, in agreement with the prescribed adiabatic boundary condition.

Figure 3 also presents the numerical temperature profile along the x-axis for the case of a coarse mesh (mesh $= 1$). This plot provides a more detailed visualization of the temperature distribution within the domain. Near the helium channel, the temperature attains its minimum value of approximately 4.5 K,

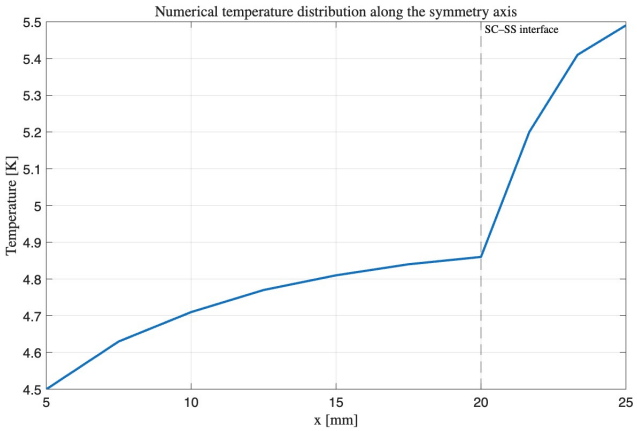

Figure 3: Computed temperature distribution mesh = 1

and it gradually increases along the x-direction, reaching a maximum of 5.49 K at the right boundary of the domain.

As expected, the plot shows a pronounced discontinuity at $x = 20$ mm, which corresponds to the physical interface within the material. This abrupt change reflects the variation in thermal conductivity at the interface, with the material beyond this point exhibiting a lower conductivity. Consequently, the temperature gradient becomes steeper across the interface, highlighting the direct influence of the material properties on the local thermal response.

In the absence of an analytical solution, the accuracy of the obtained results is assessed through additional simulations employing progressively refined meshes. For a clearer comparison, Figure 4 presents the numerical temperature distributions along the x-axis for three different mesh densities. The discrepancy among the various solutions is negligible, indicating excellent consistency. Therefore, it can be concluded that the solution obtained with the initial mesh (mesh = 1) can be considered already converged with respect to the theoretical temperature values, as further mesh refinement does not produce appreciably different results.

Regarding the heat flux, a comparison between the colormap shown in Figure 5 (corresponding to the results obtained with a mesh of 10) and that reported in Figure 2b reveals no significant discrepancies, neither qualitative nor quantitative. This observation supports the conclusion that the numerical solution obtained with the initial mesh (mesh = 1) represents a reliable and converged solution with respect to the theoretical expectations.

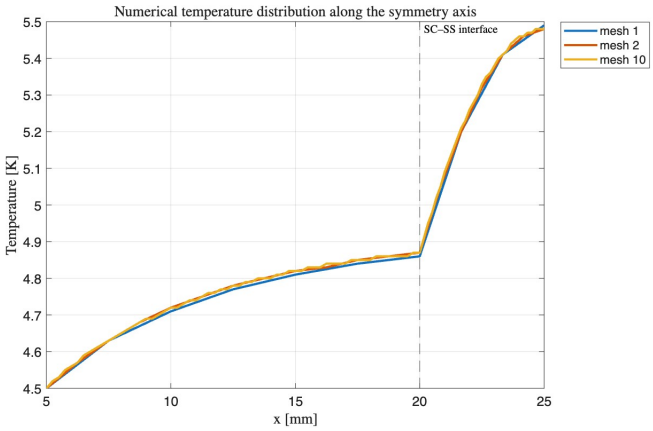

Figure 4: Computed temperature distribution along x-axes

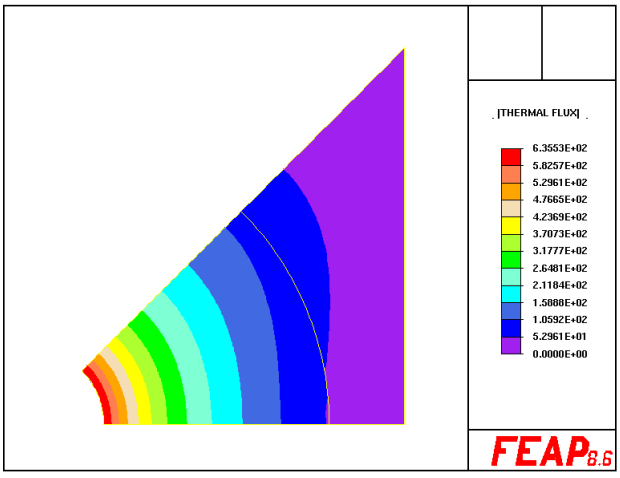

Figure 5: Computed heat flux distribution mesh=10

4 Finite Element Analysis with 4-Nodes Rectangular Elements

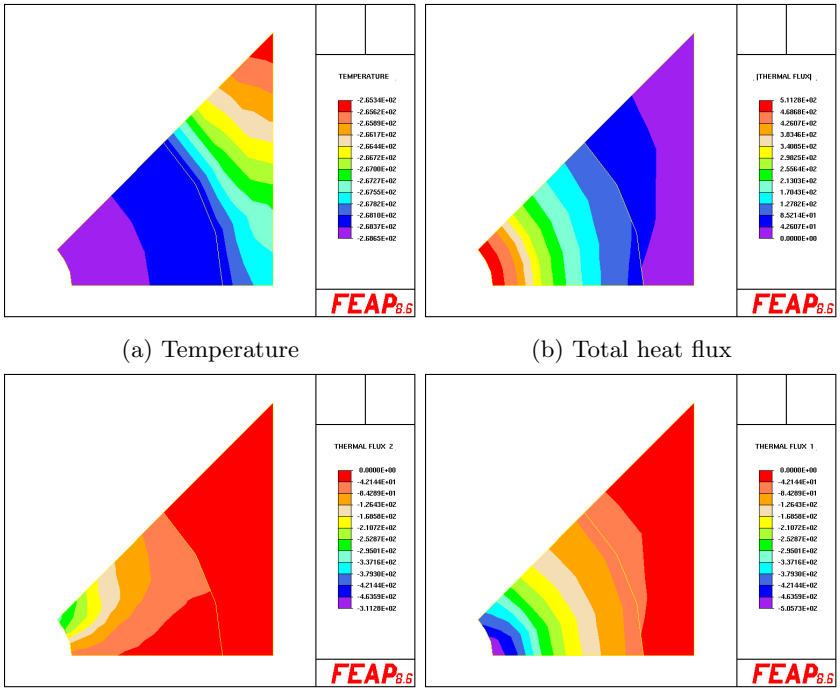

(a) Temperature (b) Total heat flux

(c) Vertical heat flux (d) Horizontal heat flux

Figure 6: Computed temperature and heat flux with mesh =1

The same analysis is now repeated using a discretization based on linear rectangular elements, following the same procedure described in Section 3. The initial results are presented in Figure 6. From Figure 6a, it can be observed that the temperature at the left boundary coincides with the helium temperature (4.5 K). The other panels, showing the total heat flux and its vertical and horizontal components, indicate zero flux at the right boundary, consistent with the adiabatic boundary condition. A brief comparison with the colormaps in Figure 2 reveals no significant discrepancies for any of the analyzed parameters; in fact, there are clear similarities both qualitatively and quantitatively. Therefore, prior to comparing these results with solutions obtained using finer meshes, it can be hypothesized that, even in this case, the numerical solution with mesh = 1 provides a sufficiently accurate approximation of the theoretical result.

Comparing the temperature distributions along the axis obtained using different mesh refinements, a clear discontinuity is observed at $x = 20$ mm, corresponding to the physical discontinuity in the material properties specified in the

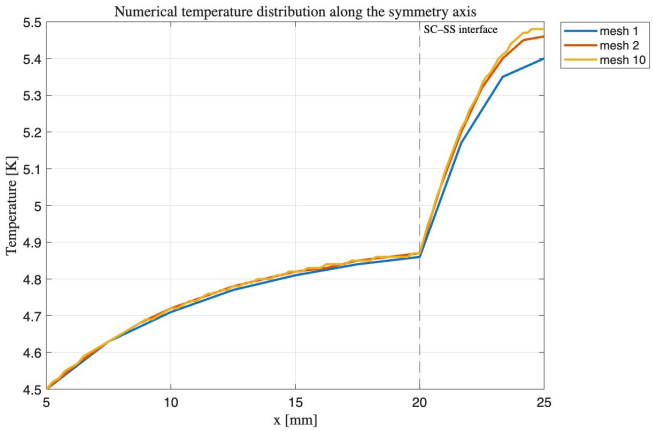

Figure 7: Computed temperature distribution along x-axes

problem. This discontinuity is associated with a sudden change in thermal conductivity, which is correctly captured by all the numerical solutions. Similarly to the observations reported in Section 3, the differences between the temperature profiles obtained with increasingly refined meshes are minimal, indicating that mesh refinement has a very limited effect on the numerical solution. Therefore, we can confidently conclude that even the solution computed using a mesh of 1 already provides an accurate representation of the temperature field, effectively capturing both the physical discontinuities and the overall thermal behavior of the domain. This demonstrates the robustness and convergence of the employed finite element discretization for the present problem.

5 Conclusion

The numerical results obtained using both 3-node triangular and 4-node rectangular elements show excellent agreement with the expected physical behavior. In particular, the temperature along the x-axis consistently exhibits a discontinuity at $x = 20$ mm, reflecting the interface between the superconducting cable and the surrounding stainless steel jacket, where the thermal conductivity changes abruptly.

A systematic comparison of the temperature profiles obtained with different mesh densities reveals that, for both element types, further refinement beyond a mesh size of 1 results in negligible differences. This observation confirms that the numerical solutions have already reached convergence with respect to the theoretical temperature distribution. In other words, the solution with mesh = 1 is sufficiently accurate to capture both the quantitative temperature values and the qualitative features of the thermal field, including the discontinuity at the material interface and the gradual increase of temperature towards the outer boundary.

Furthermore, the heat flux distributions, including their vertical and horizontal components, exhibit consistent patterns across different meshes, with zero flux at the adiabatic boundary and correct magnitude near the helium channel. This demonstrates the reliability of the finite element discretization in representing the physical phenomena and validates the assumptions made regarding symmetry and domain reduction.

Overall, these results indicate that the chosen modeling approach and the employed discretizations provide a robust and convergent numerical solution for the steady-state thermal analysis of the CICC cross-section, allowing confident interpretation of both temperature and heat flux distributions for design or experimental purposes.